EPJ E
Soft Matter and Biological Physics
EPJ.org
your physics journal

Eur. Phys. J. E **30**, 333–340 (2009) DOI: 10.1140/epje/i2009-10525-4

Criticality in a non-equilibrium, driven system: Charged colloidal rods (fd-viruses) in electric fields

K. Kang and J.K.G. Dhont

EDP SCIENCES
Società Italiana di Fisica
Springer

Eur. Phys. J. E **30**, 333–340 (2009)
DOI 10.1140/epje/i2009-10525-4

THE EUROPEAN PHYSICAL JOURNAL E

Regular Article

Criticality in a non-equilibrium, driven system: Charged colloidal rods (fd-viruses) in electric fields

K. Kang[a] and J.K.G. Dhont

Forschungszentrum Jülich, Institute für Festkörper Forschung (IFF), Weiche Materie, D-52425 Jülich, Germany

Received 22 April 2009 and Received in final form 10 July 2009
Published online: 27 October 2009 –

Abstract. Experiments on suspensions of charged colloidal rods (fd-virus particles) in external electric fields are performed, which show that a non-equilibrium critical point can be identified. Several transition lines of field-induced phases and states meet at this point and it is shown that there is a length- and time-scale which diverge at the non-equilibrium critical point. The off-critical and critical behavior is characterized, with both power law and logarithmic divergencies. These experiments show that analogous features of the classical, critical divergence of correlation lengths and relaxation times in equilibrium systems are also exhibited by driven systems that are far out of equilibrium, related to phases/states that do not exist in the absence of the external field.

PACS. 64.60.-i General studies of phase transitions – 82.70.Dd Colloids – 87.50.-a Effects of electromagnetic and acoustic fields on biological systems

1 Introduction

The divergence of thermodynamic quantities and relaxation times at equilibrium critical points is well understood, and led to the development of renormalization group theory. Universality classes have been identified that comprise many seemingly different types of systems, ranging from magnetic, ferroelectric materials and liquid mixtures to biological systems, for which divergencies with identical critical exponents are found. There are recent developments on critical phenomena in systems that are out of equilibrium. A few examples are the kinetic approaches of critical phenomena in granular materials [1], dynamical Ising models for magnetic systems [2–4] and non-equilibrium dynamical extensions of the standard C- and D-models [5]. These approaches either describe critical behavior of systems that are taken slightly out of equilibrium or relate to dynamical models that are specific for particular systems. For systems that are far out of equilibrium, there is no consensus on whether universality classes can be defined or whether every different system needs its own specific analysis. The classification of several "types of non-equilibrium" and their possible universal behavior is still under debate [6–9].

One may ask whether critical points can be associated to external-field–induced, far-out-of-equilibrium phase/state transitions, where length-scales and characteristic time constants diverge. We recently found that several phases and dynamical states in suspensions of charged colloidal rods can be induced by alternating external electric fields [10]. These new phases and states are the result of field-induced deformation of the electric double layer surrounding the rods, which affects inter-colloidal interactions. It is the purpose of the present study to show that a non-equilibrium critical point can indeed be identified in this case, with a diverging length- and time-scale.

Suspensions of fd-virus particles at low ionic strength are used as a model system for charged colloidal rods. Contrary to the phase behavior at high ionic strength [11,12], we found an isotropic-to-*non*-chiral nematic transition in the absence of an electric field at the low ionic strength that is used in the present experiments. This is probably due to the relatively large extent of the electric double layer (the Debye length is 27 nm) that surrounds the cores of the fd-virus particles, which screens the chiral structure of the fd-virus core. There are recent developments where the interaction between two colloidal rods through the polarization of their condensed layers of ions [13,14] and through electro-osmotic flows is analyzed [15]. These recent theories, however, are still far from being able to explain the phase/state behavior that we find experimentally.

This paper is organized as follows. In sect. 2, a brief description of the fd-virus system and the electrical cell is given, and the non-equilibrium electric phase/state diagram will be shortly discussed in sect. 3 (a more detailed description can be found ref. [10]). The critical divergence of the length- and time-scale are presented in sects. 4

[a] e-mail: k.kang@fz-juelich.de

and 5, respectively. An overview of the critical behaviour and a discussion are given in sect. 6.

2 Experimental details: fd-virus suspensions and the electrical cell

We use fd-virus suspensions as charged colloidal rods in external electric fields. The suspensions of bare fd-particles are prepared from the biological protocol described in ref. [16]. The fd-viruses have a length of 880 nm and a core diameter of 6.7 nm, with a persistence length of 2.5 μm. The bare surface charge of fd-virus particles is approximately $-8700\,e$ at pH = 6.9 [17]. The effective aspect ratio of fd-virus can be tuned through variation of the ionic strength; for lower salt concentrations, the aspect ratio becomes smaller due to the increase of the electrostatic Debye screening length. The suspensions of fd-viruses are dialyzed for 2 days against a 1.6×10^{-4} M TRIS/HCl-buffer. For such low buffer concentrations, the amount of carbon dioxide that dissolves from the air must be taken into account for the calculation of the ionic strength and pH (this is discussed in appendix D of ref. [18]). In order to investigate the response of fd-virus suspensions to electric fields by optical means, we use commercially available indium-tin-oxide (ITO) coated float glass (from Präzisions Glas Optik GmbH). The dimensions of our ITO glasses are $40 \times 70\,\mathrm{mm}^2$ with a thickness of 0.7 mm to ensure a uniform electric field throughout the sample. The sample amount is typically around 400 μl, and is loaded gently on the lower plate inside a rectangle of insulating PTFE film spacer (Armbrecht and Matthes GmbH, AR5038 and AR5038GP). The ITO glasses are then connected to a function generator (Avtech model AV-151G-B). We apply an alternating electric field of the form

$$E^{\mathrm{ext}}(t) = E_0 \cos\{2\,\pi\,\nu\,t\}, \qquad (1)$$

where E_0 is the applied field amplitude and ν the frequency. The optical morphologies are collected by polarization mode with an inverted microscope (Carl Zeiss, Axiovert 40CFL model) and a CCD camera (AxioCam Color A12-312). We have chosen a low-magnification 10× objective lens (NA 0.30 EC Plan-Neofluar) to monitor large regions of interests. Typical field of view is $214\times170\,(\mathrm{pixels})^2$ and $440 \times 310\,(\mathrm{pixels})^2$, where the size of the square pixels is 0.69 μm, respectively, for the measurement of image correlation functions and domain sizes.

3 The non-equilibrium electric phase/state diagram

The electric phase/state diagram in the field amplitude *versus* frequency plane is shown in fig. 1a for a suspension with a fd concentration of 2.0 mg/ml, together with depolarized optical morphologies of the various phases/states (a detailed description of the phase diagram and the various phases can be found in ref. [10]). The phase diagram in fig. 1a is corrected for "electrode polarization". The field amplitude E in fig. 1a is the field amplitude E_0 in eq. (1), corrected for electrode polarization. This correction is discussed in detail in ref. [19]. The full lines in fig. 1a are phase/state transition lines, whereas the dotted lines are related to gradual changes in texture and dynamics.

Without an electric field, the binodal concentrations for the isotropic-nematic coexistence region are 1.4 and 3.4 mg/ml for the given buffer concentration (1.6×10^{-4} M). The fd-concentration of 2.0 mg/ml used in the present experiments is within the bi-phasic region, where there is a coexistence between an isotropic and nematic phase in the absence of an electric field. No phase/state transitions have been observed in case the system is fully isotropic (for concentrations less than 1.4 mg/ml) or nematic (concentrations larger than 3.4 mg/ml). The precise degree of coarsening of the initial bi-phasic state does not affect the electric-field phase/state diagram. The size of the nematic domains is always between 100 and 300 μm, independent of the history of the sample. A well-defined stationary state can be induced by applying an electric field (with a certain amplitude and frequency). If the field is turned off, the system returns to isotropic-nematic phase coexistence, where N-domains are formed. The domains do not show any tendency to coalesce during a typical experimental duration (36–48 hours).

At a zero (or low) field strength, non-chiral nematic domains are visible between crossed polarizers (the white regions in the lower-right image in fig. 1a). Part of the black regions corresponds to the isotropic phase. The phase where nematic and isotropic phase coexist is referred to here as the N-phase. On increasing the field amplitude at low frequencies (less than about 300 Hz), a chiral texture appears (the lower-left image). This phase is referred to as the $N^\star$-phase. Apparently, the external field reduces the Debye screening length to an extent that the chiral structure of the cores of the fd-viruses comes into play, just like for higher ionic strengths in the absence of an electric field [11,12]. The chiral nematic is in coexistence with large, partly interconnected non-chiral nematic domains. On further increasing the field amplitude, there is a gradual transition where the non-chiral texture is "disconnected" and smaller non-chiral nematic domains are formed. This phase is denoted as the $N_D^\star$ phase (where the "D" stands for "disconnected domain"). The gradual transition from the $N^\star$ to the $N_D^\star$ phase is indicated by the lower dotted line and its typical morphology is shown in the left image in fig. 1a. On further increasing the field amplitude, the chiral-nematic texture disappears and a dynamical state exists where small non-chiral nematic domains melt and form (a snapshot of the morphology is given in the top-left image). Nematic domains melt and form "on the spot", that is, they do not displace during their melting or forming. The positions where domains melt and form seem to be quite random. The typical time-scale on which the domains melt and form is of the order of seconds, and is not related to the applied frequency, which corresponds to a much shorter time-scale. For field amplitudes just above the $N_D^\star$-to-D_s transition line, the dynamics is very slow (the typical times for melting and

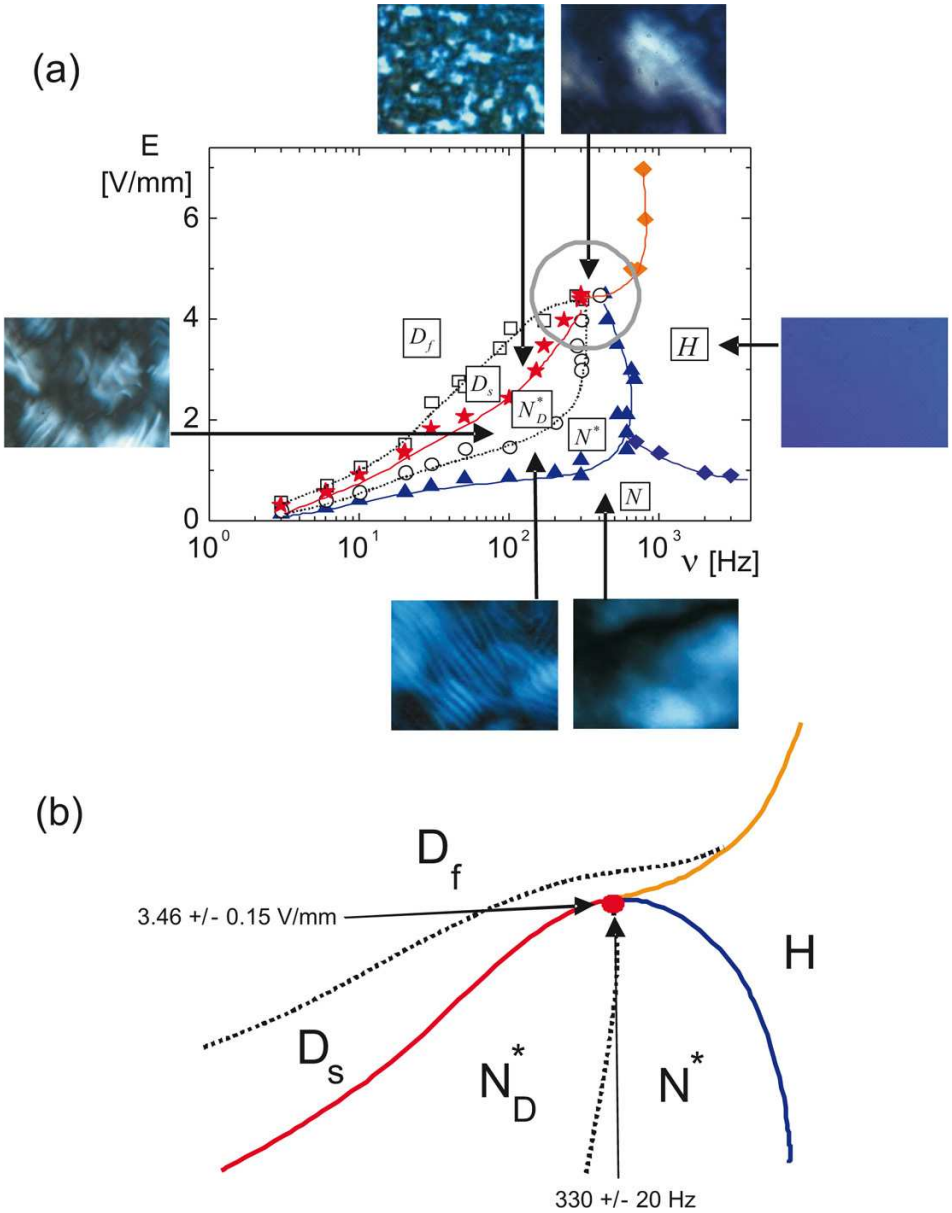

Fig. 1. (a) The phase/state diagram in the field amplitude *versus* frequency plane. At low field amplitudes there is an equilibrium between non-chiral nematic and isotropic regions; the N phase. At larger field amplitudes there is a transition (▲) to coexistence between a non-chiral nematic and chiral nematic; the $N^\star$ phase. The large non-chiral domains break up to smaller, disconnected domains in the $N^\star_D$ phase (○). The chiral texture disappears and the non-chiral nematic domains melt and form within the dynamical state D_s (⋆). In the dynamical state D_f, melting and forming of nematic domains is very fast (□). At high frequencies, in the H phase, the system becomes homogeneous, and the rods are aligned along the electric field. The N-phase directly transforms to the H phase at high frequency on increasing the field amplitude (blue ⧫), and the H phase transforms to a dynamical state at higher field amplitudes (orange ⧫). The images cover an area of $200 \times 170\,(\mu\text{m})^2$. (b) A schematic enlargement of the neighborhood of the critical point within the circle of (a). The accurate critical values for the field amplitude and frequency are indicated.

reforming is of the order of 10 to 30 seconds). For larger field amplitudes, the characteristic time for melting and forming becomes much smaller, and levels off to about 1 to 2 seconds, essentially independent of the field strength. The state where the dynamics is slow is referred to as the D_s state, while the state where the dynamics is fast is referred to as the D_f state. There is a gradual transition between those two dynamical states. A typical snapshot image of the D_f state is shown in fig. 1a by the upper dotted line. At higher frequencies, larger than about 600 Hz, there is a transition from the N phase to a uniform phase where the rods are aligned along the electric field. In ref. [10], the uniform phase is referred to the isotropic I-phase. Recent electric birefringence measurements, however, reveal that there is a homeotropic alignment at these high frequencies [19]. This uniform phase of rods aligned

along the electric field is referred to here as the H phase (where "H" stands for "homeotropic"). At high field amplitudes, larger than about 4.2 V/mm, the fast dynamical state transforms directly to the H phase on increasing the frequency.

To summarize, we find the following phases and states:

- N phase: coexistence of an isotropic and non-chiral nematic phase.
- $N^\star$ phase: non-chiral domains in coexistence with chiral domains.
- H phase: a homogeneous phase, where the rods are aligned along the electric field.
- $N_D^\star$ phase: same as the $N^\star$ phase, except that the non-chiral domains are significantly smaller and disconnected.
- D_s state: a dynamical state where non-chiral domains melt and reform.
- D_f state: same as the D_s state, except that the dynamics of melting and reforming of nematic domains is much faster.

The transitions between the $N^\star$ and $N_D^\star$ phase and the D_s and D_f state are smooth, gradual transitions: this is why these transition lines in fig. 1a are indicated by dotted lines. The solid lines in fig. 1a are sharp phase/state transitions. The detailed characterization of various transition lines in the electric phase/state diagram is presented in ref. [19].

As can be seen from fig. 1a, several transition lines meet in a single point. A schematic of the various transition lines that meet at the critical point is given in fig. 1b for clarity. That transition lines meet in a single point in the phase diagram is a feature that is common to critical points in equilibrium systems in which length- and time-scale diverge. As will be seen, both the size of nematic domains within the dynamical state (our length-scale) and the characteristic time for melting and forming of these domains (our time-scale) diverge at this "non-equilibrium critical point". Moreover, the off-critical divergencies at the $N_D^\star$-to-D_s transition line are weaker as compared to the non-equilibrium critical point. There is thus a close analogy between the observed non-equilibrium critical divergence of a length- and time-scale with that of equilibrium systems. Note that, since several transition lines meet at the critical point, it is feasible that this is in fact a multi-critical point. It is very well possible that a line of critical points originates from this multi-critical point. As will be seen later, the entire $N_D^\star$-to-D_s transition line (also off-critical) indeed exhibits a divergence of the time-scale on which melting and forming of nematic domains occurs. The domain size, however, remains finite on off-critical approach of this transition line, contrary to what is seen on approaching the critical point.

The critical values of the field amplitude and frequency that can be read off from the phase diagram in fig. 1a are about 4.2 V/mm and 300 Hz, respectively. The critical values as accurately determined from the experiments described in sects. 4 and 5, however, are 3.46 ± 0.15 V/mm and 330 ± 20 Hz (shown in fig. 1b). To within experimental error the critical frequency read off from the phase diagram in is accordance with the accurately determined value. There is, however, an apparent discrepancy for the critical field amplitude. The reason for this is as follows. The critical point in the phase diagram in fig. 1a has been obtained by visual observation, where the field amplitude is increased at a fixed frequency in steps of about 0.2 V/mm every 5 seconds. Critical slowing down at the critical point overestimates the critical field amplitude in the phase diagram in fig. 1a as a result of the finite observation time.

In the following sections, we discuss the determination of divergencies of the domain size and the characteristic time of melting and reforming of nematic domains.

4 Divergence of domain size

The nematic domain size in the dynamical state is obtained from a time-resolved series of depolarized microscopy images. The domain size is the maximum size that a given domain attains during its formation, just before melting sets in. Since most of these domains are not centered in the 2D field of focus, the true domain size is generally larger than the observed domain size. We therefore select the largest observed domain sizes from a time frame to represent the true domain size. The domain size for these selected images is determined from light intensity profiles, as shown in fig. 2a. Intensity profiles along cuts in the x- and y-direction are shown in the upper and right panel, respectively. The size along each cut is obtained from the distance where the transmitted intensity is equal to half of the plateau value within the domain, as indicated by the arrows in both panels in fig. 2a. The domain size is now taken equal to the average of the thus obtained linear dimensions along the cuts. The variation in the linear dimensions along cuts due to the non-sphericity of the domain geometry is typically of the order of 10%.

The variation of the domain size d on approaching the critical point at a fixed (critical) field amplitude of 3.50 V/mm by increasing the frequency is given in fig. 2b. In order to assess possible critical divergence of the domain size, both the background domain size d_b and the critical frequency ν_c must be determined. The background domain size is estimated from fig. 2b, first plot, as $d_b = (15 \pm 3)\,\mu$m. The critical frequency can be obtained from a linear extrapolation of $1/d$ as a function of frequency to 0, as can be seen from fig. 2b, middle plot. It is found that $\nu_c = (335 \pm 15)$ Hz. From the rightmost plot in fig. 2b, where $d - d_b$ is given as a function of $\nu_c - \nu$ in a double-logarithmic plot, we deduce that there is a logarithmic divergence, that is

$$d(\nu) - d_b \sim {}^{10}\log\left\{1 - \frac{\nu}{\nu_c}\right\}. \qquad (2)$$

The solid line in fig. 2c is a fit to this logarithmic divergence.

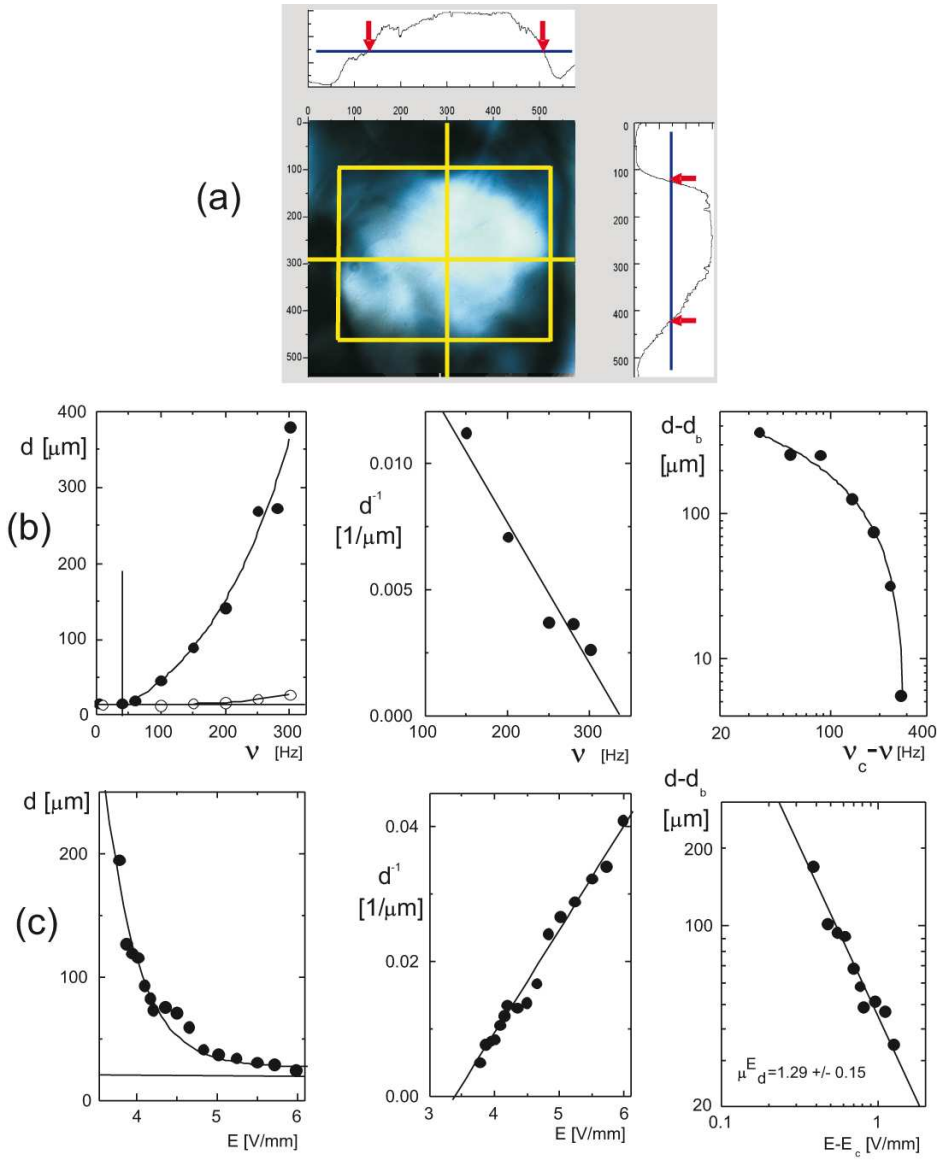

Fig. 2. Critical behavior of the domain size. (a) The determination of the domain size from microscopy images. The domain size is equal to the average of the linear dimensions along cuts through the center of the domain, which are given by the extent over which the intensity profiles decreased to half of the plateau value within the domain, as sketched in the upper and right inserts. (b) From left to right, the domain size as a function of frequency at the critical field amplitude 3.50 V/mm, the inverse of the domain size *versus* frequency to determine the critical frequency and a double-logarithmic plot that reveals logarithmic divergence. The open symbols in the leftmost figure show that the domain size remains finite for an off-critical approach of the D_s-to-$N_D^\star$ transition line at a field amplitude of 2.06 V/mm. The vertical line marks the location of the D_s-to-$N_D^\star$ transition line for this off-critical field amplitude. (c) The same as in (b), but now for variation of the field amplitude at the critical frequency of 335 Hz. The double-logarithmic plot reveals a power law divergence with a critical exponent of $\mu_d^E = 1.29 \pm 0.15$.

A comment on the linear extrapolation of the domain size as a function of frequency or field amplitude should be made for the determination of critical values, presented in the middle plots of figs. 2b and c: Using the estimated critical values, the prefactors of the logarithm or algebraic functions (as well as the critical exponent) are determined from a fit of the resulting plots on the right-hand side in figs. 2b and c. The resulting expressions for $1/d$ as a function of frequency or field amplitude are then plotted to verify whether the dependence is linear within the range of frequencies used in the linear extrapolation of experimental data. These curves turn out to be indeed linear to within typical experimental errors. This self-consistent procedure is also applied for the characteristic time constant discussed in the following section.

The domain size divergence is stronger when the critical point is approached at a fixed (critical) frequency of 335 Hz on lowering the field amplitude. The background domain size and the critical field amplitude are determined from fig. 2c as $d_b = (20 \pm 4)\,\mu$m and $E_c =$

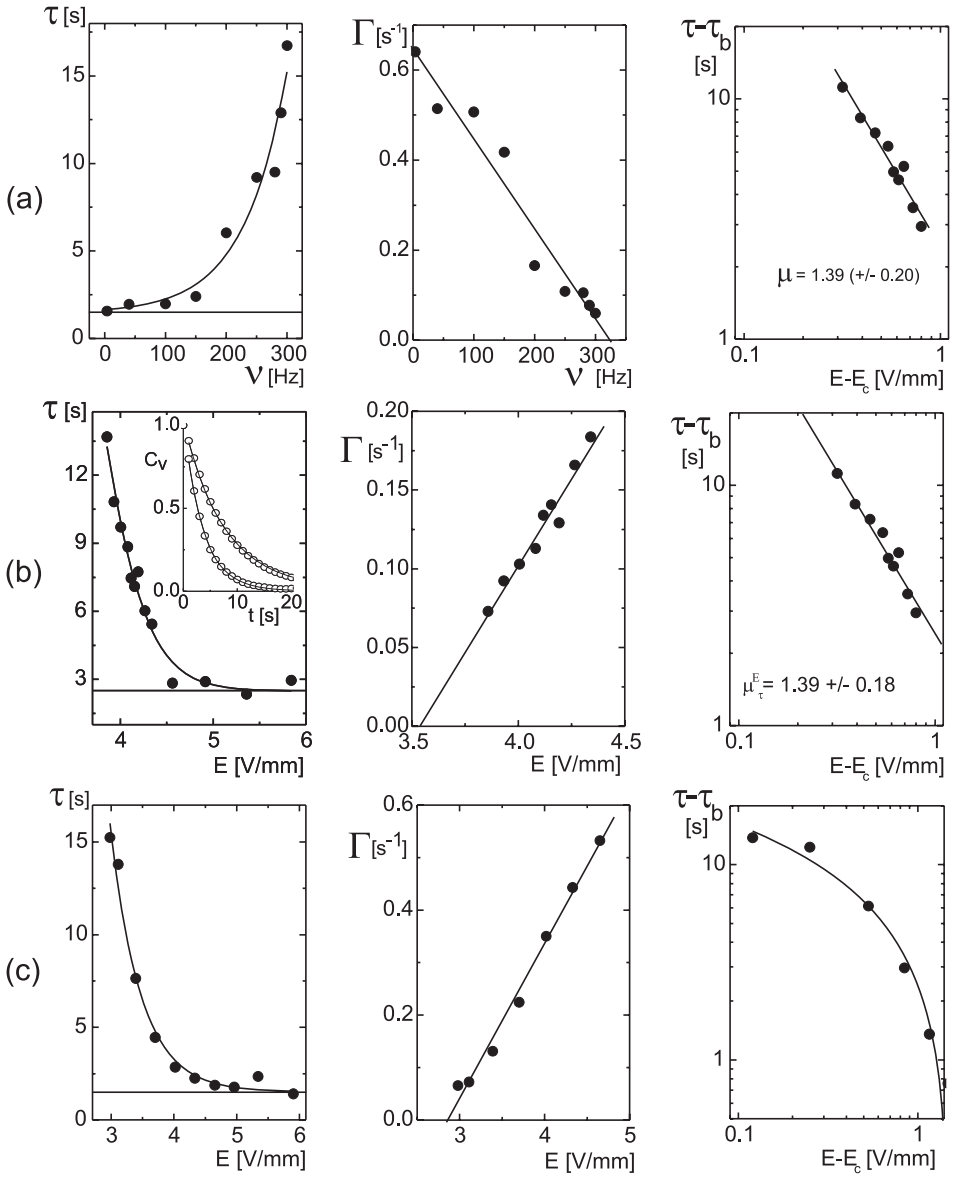

Fig. 3. Critical behavior of the time constant. (a) From left to right, the characteristic time τ for melting and forming of nematic domains, as a function of frequency at the critical field amplitude of 3.50 V/mm, the inverse $\Gamma = 1/\tau$ as a function of frequency to determine the critical frequency and a double-logarithmic plot that reveals critical divergence with an exponent equal to $\mu_\tau^\nu = 0.65 \pm 0.15$. (b) The same as in (a), but now for variation of the field amplitude at the critical frequency of 325 Hz. The double-logarithmic plot shows power law divergence with an exponent $\mu_\tau^E = 1.39 \pm 0.18$. (c) The same as in (a) and (b), but now for an off-critical approach of the D_s-to-$N_D^\star$ transition line on variation of the field amplitude at a frequency of 150 Hz. The double-logarithmic plot reveals a logarithmic divergence.

(3.40 ± 0.15) V/mm. As can be seen from the double-logarithmic plot in fig. 2c, there is a power law divergence of the domain size according to

$$d(E) - d_b \sim \left(\frac{E}{E_c} - 1\right)^{-\mu_d^E}, \qquad (3)$$

with a critical exponent $\mu_d^E = 1.29 \pm 0.15$. The extent of the D_s state above the critical point, where critical phenomena become effective, extends over a quite small field-amplitude interval. It is therefore quite difficult to obtain data in fig. 2c that extend over more than a decade.

The open symbols in the left plot in fig. 2b correspond to an off-critical approach of the D_s-to-$N_D^\star$ transition line at a fixed field amplitude of 2.06 V/mm. The vertical line marks the location of the D_s-to-$N_D^\star$ transition line at this off-critical field amplitude. Clearly, the domain size remains finite at the transition. For increasing frequencies, inside the N_D^* phase, the domain size increases to some extent, but remains finite (approximately 30 μm). Note that 2.06 V/mm and 300 Hz (the highest frequency probed for the off-critical date in the left plot in fig. 2b) is a point in the phase diagram that is far into the $N_D^\star$

phase. We always observed finite domain sizes throughout the phase/state diagram, away from the critical point.

5 Divergence of the characteristic time: Melting and formation of domains

The dynamics of nematic domains is quantified through transmitted-intensity time correlation functions as obtained from a time sequence of depolarization microscopy images, with a typical time resolution of 0.3–1 s. From such a time sequence of images, the "video-correlation function" $C_V(t)$ is obtained

$$C_V(t) = \frac{\langle [I(t) - \langle I\rangle(t)]\,[I(0) - \langle I\rangle(0)]\rangle}{\langle [I(0) - \langle I\rangle(0)]^2\rangle}\,. \qquad (4)$$

Here, $I(t)$ is the transmitted intensity for a given CCD pixel at time t, and the brackets $\langle\cdots\rangle$ denote averaging over all pixels. At each time, the pixel-average $\langle I(t)\rangle$ is subtracted from single-pixel intensities $I(t)$ in order to correct for temporal changes of the overall nematic texture. The video-correlation functions can be fitted with a stretched, single exponential function

$$C_V(t) = B + (1 - B)\,\exp\{-(t/\tau)^{\beta}\}, \qquad (5)$$

where τ defines the characteristic time-scale on which nematic domains melt and form and β is the stretching exponent. In the insert in the left plot in fig. 3b, two typical correlation functions and their fit to a stretched exponential are given.

In fig. 3a, the characteristic time τ for melting and domain formation is plotted as a function of frequency for the (critical) field amplitude 3.50 V/mm. The background value τ_b is estimated from this plot as (1.50 ± 0.25) s. The critical frequency determined from a plot of the inverse of τ *versus* frequency in fig. 3b is found to be equal to $\nu_c = (325 \pm 20)$ Hz, in accordance with the frequency where the domain size diverges. The double-logarithmic plot in fig. 3a shows that τ diverges algebraically

$$\tau(\nu) - \tau_b \sim \left(1 - \frac{\nu}{\nu_c}\right)^{-\mu_\tau^\nu}, \qquad (6)$$

with a critical exponent equal to $\mu_\tau^\nu = 0.65 \pm 0.15$. The time for melting and forming of nematic domains diverges algebraically on approaching the critical point by variation of the field amplitude (similar to the domain size in eq. (3)), with a critical exponent of $\mu_\tau^E = 1.39 \pm 0.18$. The critical field amplitude $E_c = (3.53 \pm 0.15)$ V/mm obtained from fig. 3b is in agreement with the value where the domain size diverges.

The results of off-critical measurements for τ with an approach of the D_s-to-$N_D^\star$ transition line at a fixed frequency of 150 Hz are given in fig. 3c. The background value is (1.50 ± 0.20) s, while the transition field amplitude is found to be equal to $E_t = (2.84 \pm 0.08)$ V/mm. From fig. 3c a logarithmic divergence is found (similar to eq. (2), but now for the field amplitude instead of frequency). The domain size remains finite.

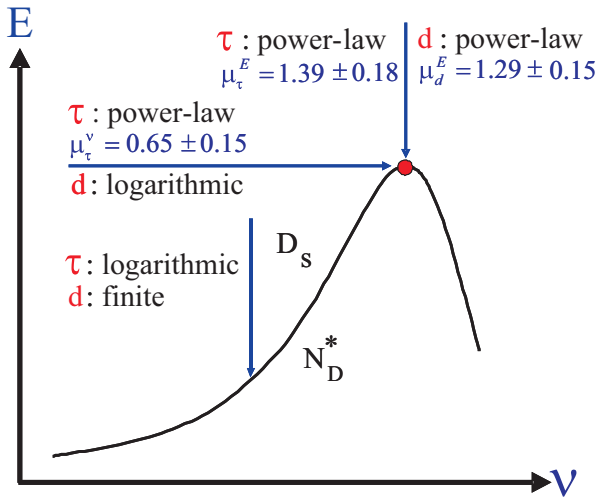

Fig. 4. A schematic overview of the critical and off-critical behavior of the domain size d and the characteristic time τ for melting and forming of nematic domains.

6 Summary and discussion

Experiments have been performed on dispersions of charged rods (fd-virus) in electric fields. The present study shows that a critical point can be identified where a length- and time-scale diverge. The length-scale is associated with the maximum size d of nematic domains in a dynamical state where the domains melt and form, while the time-scale τ corresponds to the characteristic time during which domains melt and form. Both power law and logarithmic divergencies have been found. Figure 4 is a summary of the critical behavior. Exponential behavior is found on approaching the critical point from above, on lowering the field amplitude, while both power law (for τ) and logarithmic (for d) divergencies are found on approaching the critical point by increasing the frequency. Off-critical, the characteristic time τ diverges logarithmically, more weakly as compared to its critical divergence, while the domain size remains finite.

At the $N_D^\star$-to-D_s transition line for frequencies below the critical frequency, the domain size remains finite but the characteristic time diverges weakly (logarithmically). We referred to this line as "off-critical". We can, however, not exclude the possibility that this transition line is a line of critical points in some sense.

The critical behavior found in the present study is related to phases/states that are induced by the external field. Much like for equilibrium critical points, several phase/state transition lines meet at the non-equilibrium critical point, although in the present case there are no phases that become "indistinguishable" at the critical point. The field-induced phases/states are far out of equilibrium, and yet show similar critical behavior as compared to equilibrium systems. It is unclear whether critical phenomena in driven systems are universal in the sense that universality classes can be defined, analogous to systems in equilibrium, or whether each type of driven system demands a system-specific analysis.

What has not been addressed in the present study are possible divergencies on approaching the critical point from the side of the H phase. Contrary to dynamical states, the H phase is stationary and uniform, so that it would be interesting to probe the correlation length and the dynamics in the H phase of either translational or orientational diffusion on approaching the non-equilibrium critical point. Dynamic light scattering experiments of the high-frequency H phase indeed show pronounced critical slowing down of diffusion. The microscopic dynamics in the H phase will be published in a separate paper.

Part of this research was supported by the Trans-regio SFB 6018 "Physics of Colloidal Dispersions in External Fields" and by the EU-FP7 Network "NanoDirect" (contract number CP-FP-213948-2).

References

1. E.V. Ivashkevich, A.M. Povolotsky, A. Vespignani, S. Zapperi, Phys. Rev. E **60**, 1239 (1999).
2. C. Godrèche, J.M. Luck, J. Phys.: Condens. Matter **14**, 1589 (2002).
3. L. Környei, M. Pleimling, F. Iglói, arXiv:0710.2829vl [cond-mat.stat-mech] 15 oct. (2007).
4. M. Henkel, G.M. Schütz, J. Phys. A: Math. Gen. **37**, 591 (2004).
5. V.K. Akkineni, U.C. Täuber, Phys. Rev. E **69**, 036113 (2004).
6. N. Goldenfeld, L.P. Kadanoff, Science **284**, 87 (1999).
7. H. Hinrichsen, Adv. Phys. **49**, 815 (2000).
8. G. Odor, Rev. Mod. Phys. **76**, 663 (2004).
9. S. Lubeck, Int. J. Mod. Phys. B **18**, 3977 (2004).
10. K. Kang, J.K.G. Dhont, EPL **84**, 14005 (2008).
11. Z. Dogic, S. Fraden, Curr. Opin. Colloid Interface Sci. **11**, 47 (2006).
12. E. Grelet, S. Fraden, Phys. Rev. Lett. **90**, 198302 (2003).
13. J. Ray, G.S. Manning, Langmuir **10**, 2450 (1994).
14. J. Ray, G.S. Manning, Macromolecules **33**, 2901 (2000).
15. D. Saintillan, E. Darve, E.S.G. Shaqfeh, J. Fluid Mech. **563**, 223 (2006).
16. J. Sambrook, E.F. Fritsch, T. Maniatis, *Molecular Cloning: A Laboratory Manual* (Cold Spring Harbor Laboratory, New York, 1989).
17. K. Zimmermann, J. Hagedorn, C.C. Heuck, M. Hinrichsen, J. Ludwig, J. Biol. Chem. **261**, 1653 (1986).
18. K. Kang, A. Wilk, A. Patkowski, J.K.G. Dhont, J. Chem. Phys. **126**, 214501 (2007).
19. K. Kang, J.K.G. Dhont, to be published in Soft Matter.